

Model of lens candidates from Space Warps CFHTLS

Rafael Küng,¹ Prasenjit Saha,¹ Ignacio Ferreras,² Elisabeth Baeten,³ Jonathan Coles,⁴ Claude Cornen,³ Christine Macmillan,³ Phil Marshall,⁵ Anupreeta More,⁶ Lucy Oswald⁷ Aprajita Verma⁸ and Julianne K. Wilcox⁴

¹Physik-Institut, University of Zurich, Winterthurerstrasse 190, 8057 Zurich, Switzerland

²Mullard Space Science Laboratory, University College London, Holmbury St Mary, Dorking, Surrey RH5 6NT, UK

³Zooniverse, c/o Astrophysics Department, University of Oxford, Oxford OX1 3RH, UK

⁴Exascale Research Computing Lab, Campus Teratec, 2 Rue de la Piquetterie, 91680 Bruyeres-le-Châtel, France

⁵Kavli Institute for Particle Astrophysics and Cosmology, Stanford University, 452 Lomita Mall, Stanford, CA 94035, USA

⁶Kavli Institute for the Physics and Mathematics of the Universe, University of Tokyo, 5-1-5 Kashiwanoha, Kashiwa-shi 277-8583, Japan

⁷Murray Edwards College, University of Cambridge, Cambridge CB3 0DF, UK

⁸Sub-department of Astrophysics, University of Oxford, Denys Wilkinson Building, Keble Road, Oxford, OX1 3RH, UK

22 July 2016

ABSTRACT

We report modelling follow-up of recently-discovered gravitational-lens candidates in the CFHT Legacy Survey. Lens modelling was done by a small group of specially-interested volunteers from the Space Warps citizen-science community who originally found the candidate lenses. Models are categorised according to seven qualitative and quantitative points. Also included are some improvements to the modelling software used (SpaghettiLens), and discussion of strategies for scaling to future surveys with more and frequent discoveries.

The candidates successfully modelled are all galaxies, with inferred lensing masses ranging from $\sim 10^{11} M_{\odot}$ to $> 10^{13} M_{\odot}$. Stellar masses have also been estimated, using photometry from the CFHTLS pipeline and stellar-population models. A trend well-known in nearby galaxies, that star-formation efficiency is maximal for total masses of $\approx 10^{12} M_{\odot}$ and reduces for both lower and higher masses, is discernable also in these much more distant galaxies.

Key words: gravitational lensing: strong – keyword2

1 INTRODUCTION

Light deflection at the rim of the Sun is famously $1.75''$. The deflection angle can also be expressed in terms of the escape velocity $2v_{\text{esc}}^2/c^2$, with v_{esc} at the solar surface being ≈ 620 km/s. The Galactic escape velocity at the Sun's location is similar: ≈ 500 km/s, typical of massive galaxies. Thus, the outer regions of massive galaxies have lensing deflections comparable to that at the rim of the Sun. Yet these quantitatively similar deflections have qualitatively different consequences. Light deflection by the Sun must be accounted for in modern astrometry (see e.g., Crosta et al. 2015) but is not itself a physics probe in the way it was a century ago. With distant galaxies, however, light bending by $\sim 1''$ introduces two new phenomena. First, for galaxies distant enough that their apparent size is comparable to the bending angle, light deflection can cause multiple images of background sources, or strong lensing. Second, the gravitational field is dominated by dark matter, hence strong lensing becomes a probe of dark matter in galaxies.

With no unambiguous dark-matter particle detections so far, dark matter has studied only through its indirect consequences on galactic and larger scales. In most work, dark matter is taken to be a collisionless non-relativistic fluid (cold dark matter or CDM); in recent years, the simulation by Springel et al. (2005) has been particularly influential in studying the formation of CDM structures. Other scenarios have also been considered, such as a cold condensing boson fluid (Schive et al. 2016). There is a general consensus, however, that the origins of galaxy lie in the gravitational collapse, fragmentation, and mergers of dark-matter clumps, into which fell gas, cooling through radiative processes to form dense clouds and eventually stars. There is, however, much debate about the details, of which Silk & Mamon (2012) provide a nice summary.

Strong-lensing galaxies are a useful source of information on the mutual dynamics and dark matter and gas in galaxies. The topic has been explored in several studies (Koopmans et al. 2009; Leier et al. 2011, 2012, 2016; Bruderer et al. 2016)

but it is desirable to enlarge the samples from tens of lensing galaxies to thousands. Doing so requires finding more lenses, of course, but also modelling their masses.

Recent searches through the CFHTLS (Cuillandre et al. 2012) using arc-finders (More et al. 2012; Maturi et al. 2014; Gavazzi et al. 2014) by machine learning (Paraficz et al. 2016) and by visual inspection by a citizen-science volunteers (Space Warps More et al. 2016) have between them discovered an average of four lenses per square degree. So one can be optimistic about finding many thousands of lenses in the next generation of wide-field surveys. The expected flood of new lens discoveries will need a similarly huge modelling modelling effort to reconstruct their mass distributions. To prepare for the challenge of massive-sample lens modelling, Küng et al. (2015) developed a new modelling strategy, implemented as the SpaghettiLens system. The idea is to collaborate with experienced members of the citizen-science community, who have already participated in lens discovery through Space Warps, as well as several other projects involving astronomical data. In this paper, we present SpaghettiLens models of lens-candidates discovered through Space Warps.

Section 2 summarises the SpaghettiLens system and discusses its ongoing development. A SpaghettiLens model consists of a statistical ensemble of free-form maps of the sky-projected mass distribution responsible for lensing. Each lens candidates in practice gets modelled several times in a collaborative refinement process¹ In this paper we report the most recent model for each lens, as representing a consensus among modellers, as to the best that could be achieved with the available data and software. Photometric lens redshifts are used; source redshifts are set to $z = 2$. The models can, however, be trivially rescaled to use better redshift values, as and when they become available. Küng et al. (2015) tested the system on simulated lenses and identified some areas for improvement. The first two of those are taken up in Section 2, along with a further idea. In § 2.1 we introduce fitting of the brightness profiles of the source. This feature has not yet been included in SpaghettiLens, but has been carried out in post-processing for a few especially interesting candidates. In § 2.2 we show that making mass maps fine-grained in the central region relieves a tendency in the earlier work for mass to be too shallow. Then in § 2.3 we consider the possibility of fitting a parametric lens model to the model ensemble; so far we have only been successful at extracting an Einstein radius.

Section 3 explains how we compare the lensing mass with the mass in stars in the lensing galaxy. We estimate the stellar mass by comparing galaxy magnitudes from the CFHTLS pipeline with the well-known stellar-population models of Bruzual & Charlot (2003). We then extrapolate the stellar masses to a halo mass using the abundance-matching prescription of Moster et al. (2010). Naturally, the lensing mass must be more than the stellar mass but no more than the total halo mass. We then introduce what we call a halo index \mathcal{H} which gives an idea of how the lensing mass compares with these two bounds.

Section 4 discusses ten of the systems, including six

¹ See ‘‘Collaborative gravitational lens modelling...’’ in <http://letters.zooniverse.org> especially the model tree.

systems we found to be particularly interesting. The online supplement gives results for all the modelled systems.

In Section 5 and Table 1 we display a concise characterisation of each modelled system, according to the image morphology and how clear or indistinct it is, whether the mass map and synthetic lensed image appear to be plausible, and how the model mass compares with the estimated stellar and full-halo masses.

2 LENS MODELLING

SpaghettiLens is an example of a medium-sized collaboration spawned by a large citizen-science project (in this case Space Warps). While collaboration with volunteers is essential to both, the form of collaboration is very different. In Space Warps, volunteers in a crowd of $\gtrsim 10^4$ make independent contributions. Each person is presented with a random selection of survey-patches and invited to (in effect) vote on each. The system estimates each volunteer’s skill level according to test-patches interspersed with the real data, and weights their votes accordingly (Marshall et al. 2016). There is an active forum for volunteers, but since everyone is seeing different data samples with minimal overlap, the forum has little if any influence on votes. With SpaghettiLens, on the other hand, there is a small group of volunteers and their contributions are interdependent.

A modeller’s main input to SpaghettiLens is a sketch of arrival-time contours on a lensed system. It gives the locations (or best-guess locations) of images of point-like sources, along with their ordering in arrival time, and their parities (minimum, saddle-point or maximum). Such a sketch, which we call a spaghetti diagram, tends to resemble the form of lensed arcs, but it also in effect encodes a proposal for its mass distribution. A spaghetti diagram is read by a server-side numerical engine (GLASS, developed by Coles et al. 2014) which then returns a statistical ensemble of mass maps. The mass maps are made up of mass tiles and are free-form, except that they are required to be concentrated around the identified lens centre. They are also required to reproduce the given image locations, parities and time ordering exactly. Graphical representations of the mass map and arrival-time surface are returned to the user for review. The user can post these results on a forum, or discard them and try again. Volunteers can start the modelling process afresh, or they can take an existing model from the forum and modify its input spaghetti diagram or its accompanying options, and thus obtain a revised model.

2.1 Improved synthetic images

The mass maps produced by current implementation of SpaghettiLens are based on images of point-like features. No information about extended images is used, except in so far as they help the user identify images of point-like features. The synthetic images offered to users are rudimentary, based on sources with conical light profiles.

We have now developed a prototype of better way to generate synthetic images. Figure 1 illustrates. First, areas containing lensed images are selected (green frames in the figure). The selected areas must contain no light from the lensing galaxy or from extraneous objects. Pixels within the

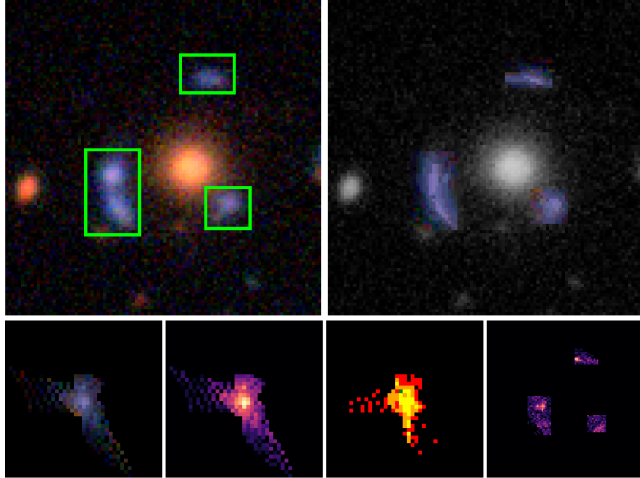


Figure 1. Synthetic lensed image with source-profile fitting in SW05 (J143454.4+522850). Top-left: original image, with areas containing lensed images enclosed within green frames. Top-right: synthetic image (coloured arcs) with lensing galaxy and unrelated objects in greyscale. Bottom from left to right: reconstructed source in colour, intensity (greyscale), count of lens plane pixels per source plane pixel, residual of original image to synthetic image.

selected areas are mapped to a grid on the source plane, using bending angles given by the mass model. The mapping from lens-plane pixels to source-plane grid cells is many-to-one, because of image multiplicity and magnification. The brightness of each source-plane pixel is set to the mean of all the lens-plane pixels mapping to it. Finally, the mapping is run back to the lens plane. The result is a synthetic image. In effect, one is reconstructing a source-plane brightness map by least-squares.

The procedure is not yet implemented in SpaghettiLens but can be applied in post-processing. The new synthetic images could be used to improve the mass reconstruction, by weighting the ensemble of maps according to how good the synthetic images are, but we have not attempted to do so as yet.

2.2 Sub-sampling of central region

In a previous paper Küng et al. (2015) we identified the problem of the tendency of the models to be too shallow. We pinned down the problem to the central region and are confident to have it fixed with enabling sub pixel sampling in the central area. The software allows for subsampling parameters of radius of pixels r_{subs} and amount of subpixels per pixel n_{subs} . Figure 2 shows the results of different settings for r_{subs} and n_{subs} . We can see that even the computationally least expensive settings of $r_{\text{subs}} = 1$ and $n_{\text{subs}} = 3$ leads to drastically improved profiles.

2.3 Parameterisation of pixel models

In order to fit the set of pixelated models to a single parameterised model, a program was written that took a parameterised function and subtracted from it the mean and the principle components of the data, which were calculated

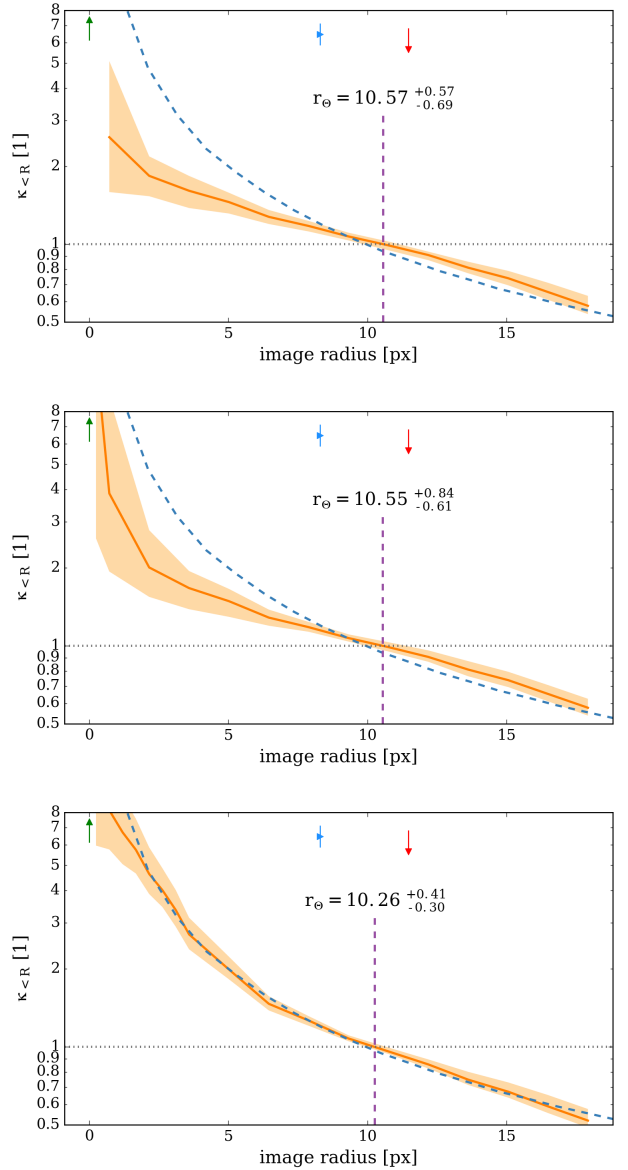


Figure 2. Same sim as in Figure 3 in the earlier paper.

using classical Principle Component Analysis. This created the residuals function. The number of components defined as principle was varied to test how this affected the output, and it was found that using 5 principle components tended to give a reasonable approximation. A masking function was added which selected only the data points that fell inside the image of the lens, and the principal components were clipped in order to keep the values inside the region of the ensemble of models. Any value higher than the clip was set to be the clip value. This was chosen to be 2.5 as, assuming that the data follows a Gaussian error distribution, almost all the values for the variance should lie between 2 and 3 standard deviations from the mean. Minimising the residuals function produces the set of parameters that fit the parameterised function to the original pixelated ensemble most closely. A least squares fit was used to perform this minimisation. The parameterised model function was obtained from the gravitational potential

of an isothermal ellipsoid mass distribution Keeton (2001). This model is frequently used to describe gravitational lenses as it tends to fit well with observations. The isothermal ellipsoid model outputs three useful parameters: the radius of the Einstein ring, the ellipticity of the model and the angle of the ellipticity from the vertical, giving the orientation of the galaxy. By applying this model to simulated lenses for which the values of these parameters were already known, it was possible to gain an estimate of the projected accuracy of the results, before applying the model to the candidate lensing galaxies.

3 STELLAR MASS

Based on Bruzual & Charlot (2003) models.
Following Moster et al. (2010)

$$\frac{M_{\text{stel}}}{M_h} = \frac{2C_0}{(M_h/M_1)^{-\beta} + (M_h/M_1)^\gamma} \quad (1)$$

$$C_0 = 0.02820, \quad M_1 = 10^{11.884} M_\odot$$

$$\beta = 1.057, \quad \gamma = 0.556.$$

$$\mathcal{H} = \frac{\ln(M/M_{\text{stel}})}{\ln(M_h/M_{\text{stel}})} \quad (2)$$

which we may call the halo-matching index.

- $\mathcal{H} < 0$ is unphysical because $M < M_{\text{stel}}$.
- $\mathcal{H} = 0$ is when the stellar mass exactly accounts for the lensing mass.
- $0 < \mathcal{H} < 1$ is the typical situation, where the lens includes stars and dark matter, but not the full halo.
- $\mathcal{H} = 1$ means that the lens consists of the entire halo.
- $\mathcal{H} > 1$ is in tension with abundance-matching, because the lensing mass exceeds the expected halo mass.

4 EXAMPLE SYSTEMS

In this section we show modelling results for ten of the lens candidates. The first five (see Figures 3–7) are the most convincingly modelled systems. The next three cases (Figures 8–10) are less good but still very plausible models, and are representative of the majority of the sample. The last two are examples where the models were unconvincing (Figures 11) or completely failed (12).

Let us first consider Figure 3, which shows model results from SW05 (J143454.4+522850).

(i) In the upper row we have first a cutout of the Space Warps image, marked up with a spaghetti diagram. There are four distinct lensed images, and the spaghetti diagram proposes that they are a minimum nearest to the lensing galaxy, a close minimum-saddle pair, and a minimum further away. In Table 1 we refer to such configurations as IQ for inclined quad.

(ii) Alongside is a synthetic image produced by modelling. In it, the fitted lensed images are shown in colour, while the lensing galaxy and extraneous objects have been reduced to grayscale. (Figure 1 in § 2.1 shows a synthetic image from another model of the same system.) These two panels are qualitative and display no units, and moreover, the mutual alignment of the two panels is only approximate.

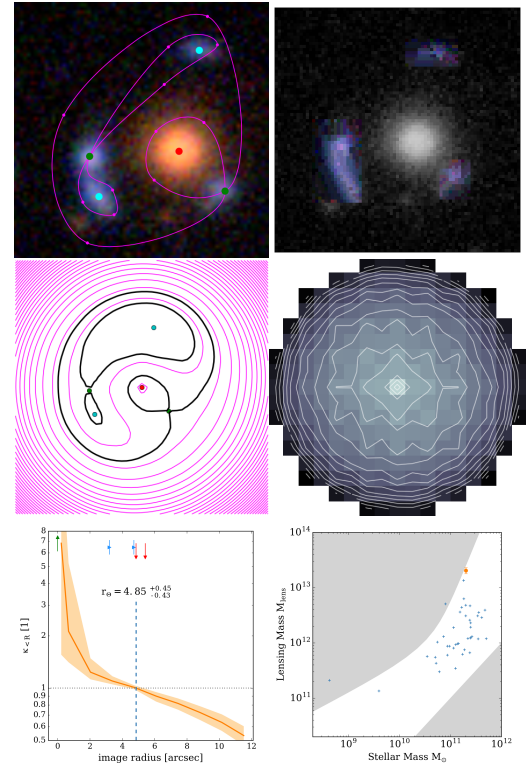


Figure 3. Model results for SW05 (J143454.4+522850). See text in Section 4 for details.

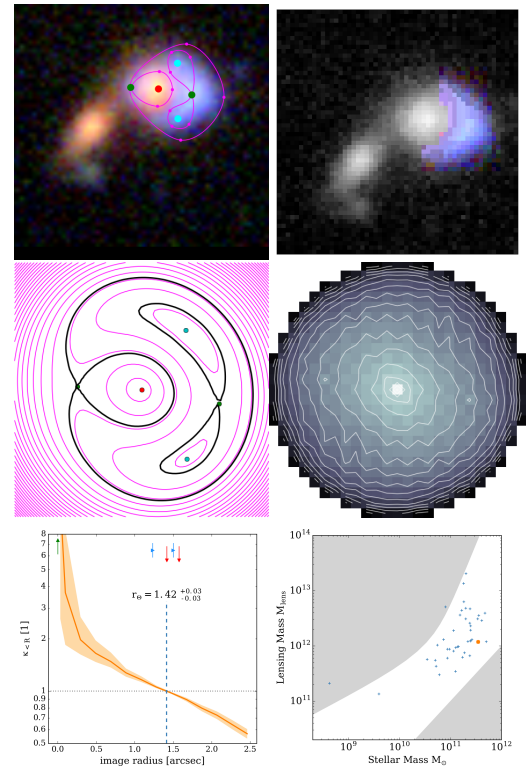
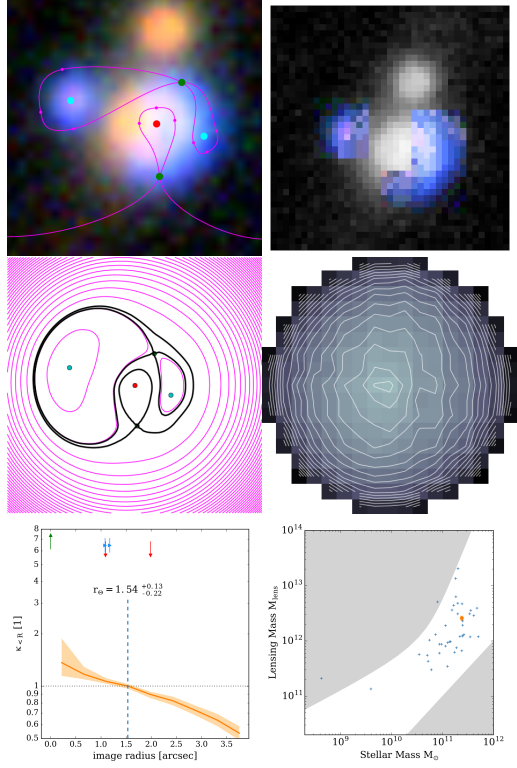
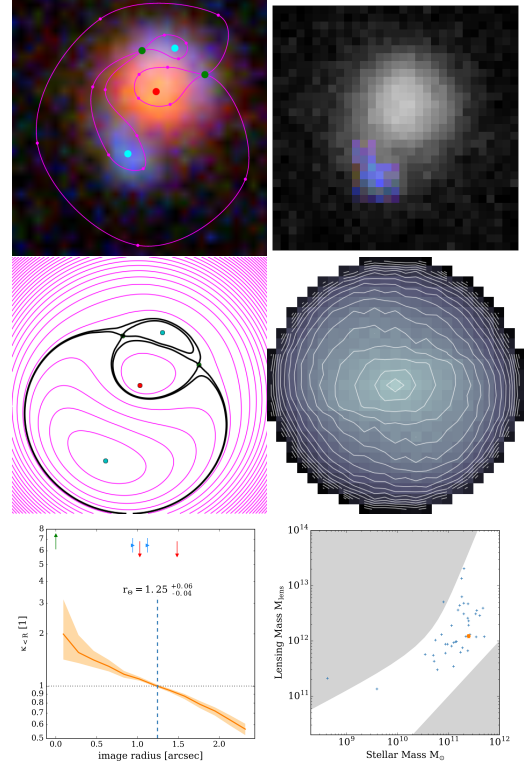
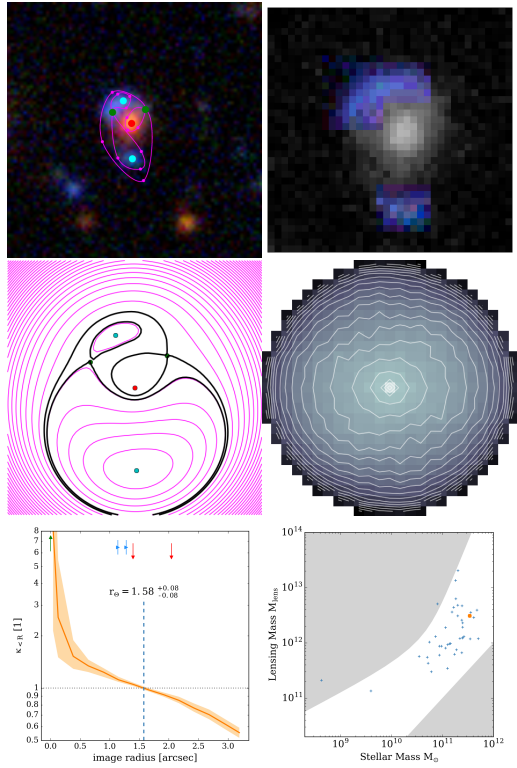
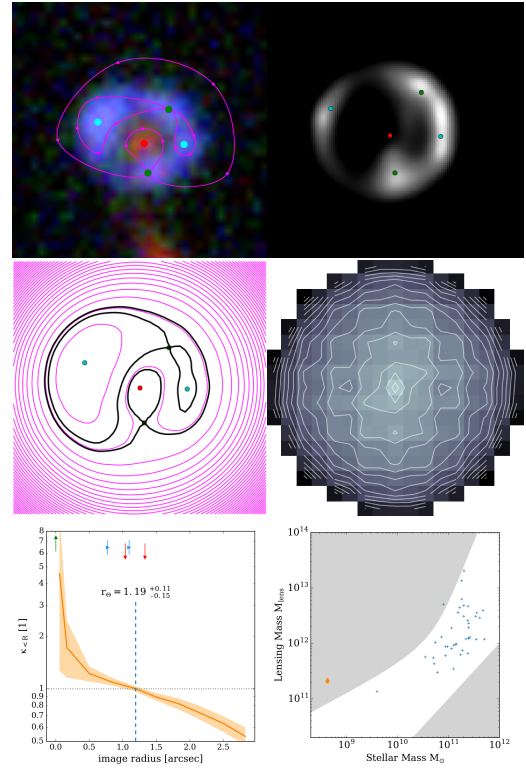
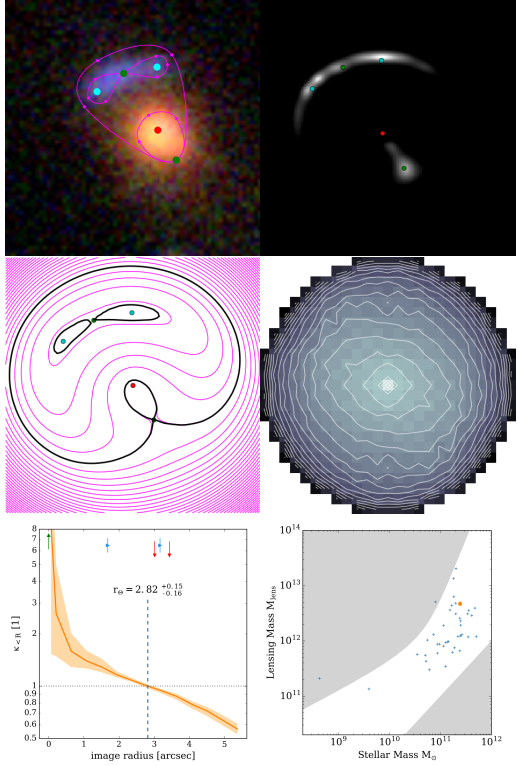
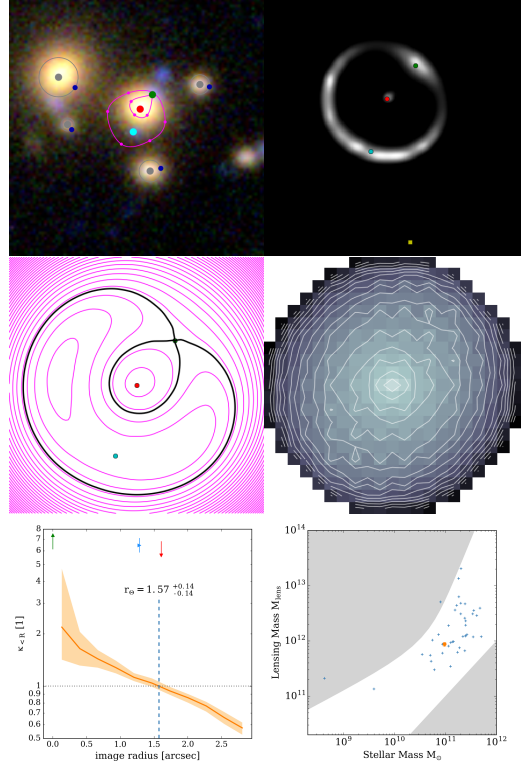
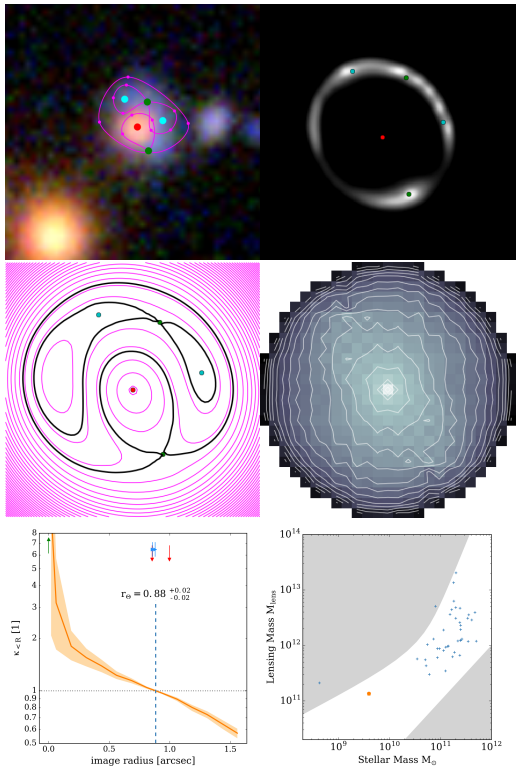
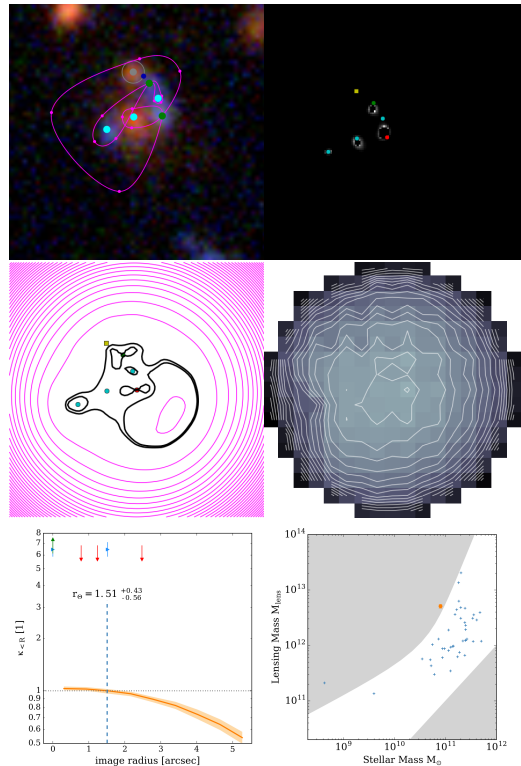


Figure 4. Model results for SW28 (J143055.9+572431).

**Figure 5.** Model results for SW02 (J140522.2+574333).**Figure 7.** Model results for SW29 (J143838.1+572647).**Figure 6.** Model results for SW09 (J020832.1-043315).**Figure 8.** Modelling results for SW42 (J221716.5+015826).

**Figure 9.** Model results for SW58 (J143651.6+530705).**Figure 11.** Model results for SW36 (J090248.4-010232).**Figure 10.** Model results for SW19 (J020642.0-095157).**Figure 12.** Model results for SW57 (J143631.5+571131).

(iii) The middle row shows contour maps from the model. At middle left, we have the arrival-time surface.

(iv) At middle right we have the mass distribution in the usual dimensionless form κ . Again, these two panels are mainly qualitative: both panels are spatially registered and centred on the density-peak of the lens, but no scales have been included.

(v) The base row supplies spatial and mass scales. The left panel shows the circularly-averaged κ of the model ensemble, with increasing radius (in arcsec). The four short vertical lines correspond to the minima and saddle points marked in the upper-left panel. The effective Einstein radius is also shown. As the radius scale indicates SW05 is comparatively large lens on the sky.

(vi) Lower right shows the total mass in the model against the estimated stellar mass, alongside the values for the whole sample. The lower-right shaded region is unphysical according to the stellar-population models, because it gives $M < M_{\text{stel}}$. The upper-left shaded region is unphysical according to abundance matching, because it gives $M > M_{\text{h}}$. That is to say, the unshaded region is $0 < \mathcal{H} < 1$.

Proceeding to Figure 4, we have one image close to the galaxy and an arc further away, which is interpreted as a blend of three images (a saddle point with two minima on either side). We call this a long-axis quad or LQ configuration. It is an indication of a mass distribution elongated along the arc-counterimage direction (along EW in this case).

In Figures 5–7 we see three candidates with an arc close to the lensing galaxy and one image further away. The arc is interpreted three images (a minimum with two saddle points on either side). We call this a short-axis quad or SQ configuration. It is an indication of a mass distribution elongated perpendicular to the arc-counterimage direction.

Figures 5–7 (SW05, SW28, SW02, SW09 and SW29) all correspond to the mass range of massive ellipticals. SW05 is the most massive of all the candidates, with a galaxy-group scale mass.

Figure 8 shows SW42. The image morphology is similar to SW05 in Figure 3, but the lens is much smaller on the sky, and the inferred mass is at the low end of the sample. (The synthetic image shown is cruder than for the five previous figures, but that does not influence the mass models.) If these preliminary findings are confirmed by follow-up observations, this could be the most dark-matter dominated lens known.

Figures 9 and 10 appear plausible lens candidates. Their morphology is similar to SW28, but the saddle-point counterimage is not visible. We consider these lenses plausible but less convincing.

Figures 11 and 12 are cases where modelling failed.

5 SUMMARY OF MODELS

Table 1

(i) The image morphology concisely described: D for double, and quads in sub-categorised in four ways (cf. Saha & Williams 2003) as LQ for long-axis quads (as in Figure 4), SQ for short-axis quads (as in Figure 5, 6, 7, 8), IQ for inclined quads (as in Figure 3) and CQ for very symmetric core quads.

(ii) Whether the images are unblended. Distinct unblended

images (as in Figures 3 and 8) are an advantage in modelling, but not essential.

(iii) Whether all images are discernable. The topography of an arrival-time surface, as encoded by a spaghetti diagram, may require more images than are visible. For example, in Figure 9, the modeller has put in a conjectural saddle point near the lensing galaxy.

(iv) Whether the lens is fairly isolated.

(v) Whether the arrival-time surface and synthetic image are plausible. In Figure 11 the model implies extra images or a long arc, which are not seen.

(vi) Whether the mass map is reasonable.

(vii) The halo index \mathcal{H} .

REFERENCES

- Bruderer C., Read J. I., Coles J. P., Leier D., Falco E. E., Ferreras I., Saha P., 2016, *MNRAS*, **456**, 870
 Bruzual G., Charlot S., 2003, *MNRAS*, **344**, 1000
 Coles J. P., Read J. I., Saha P., 2014, *MNRAS*, **445**, 2181
 Crosta M., Vecchiato A., de Felice F., Lattanzi M. G., 2015, *Classical and Quantum Gravity*, **32**, 165008
 Cuillandre J.-C. J., et al., 2012, in Observatory Operations: Strategies, Processes, and Systems IV. p. 84480M, doi:10.1117/12.925584
 Gavazzi R., Marshall P. J., Treu T., Sonnenfeld A., 2014, *ApJ*, **785**, 144
 Keeton C. R., 2001, ArXiv: astro-ph/0102341,
 Koopmans L. V. E., et al., 2009, *ApJ*, **703**, L51
 Küng R., et al., 2015, *MNRAS*, **447**, 2170
 Leier D., Ferreras I., Saha P., Falco E. E., 2011, *ApJ*, **740**, 97
 Leier D., Ferreras I., Saha P., 2012, *MNRAS*, **424**, 104
 Leier D., Ferreras I., Saha P., Charlot S., Bruzual G., La Barbera F., 2016, *MNRAS*, **459**, 3677
 Marshall P. J., et al., 2016, *MNRAS*, **455**, 1171
 Maturi M., Mizera S., Seidel G., 2014, *A&A*, **567**, A111
 More A., Cabanac R., More S., Alard C., Limousin M., Kneib J.-P., Gavazzi R., Motta V., 2012, *ApJ*, **749**, 38
 More A., et al., 2016, *MNRAS*, **455**, 1191
 Moster B. P., Somerville R. S., Maulbetsch C., van den Bosch F. C., Macciò A. V., Naab T., Oser L., 2010, *ApJ*, **710**, 903
 Paraficz D., et al., 2016, preprint, ([arXiv:1605.04309](https://arxiv.org/abs/1605.04309))
 Saha P., Williams L. L. R., 2003, *AJ*, **125**, 2769
 Schive H.-Y., Chiueh T., Broadhurst T., Huang K.-W., 2016, *ApJ*, **818**, 89
 Silk J., Mamon G. A., 2012, *Research in Astronomy and Astrophysics*, **12**, 917
 Springel V., et al., 2005, *Nature*, **435**, 629

neck
notomy
of
is can-
date.

Table 1. Categorisation of SW models

SWID	ASW id	model id	z_{lens}	image morphology	unblended images	all images discernible	isolated lens	synthetic image reasonable	mass map reasonable	total vs stellar mass ratio
SW01	ASW0004dv8	J022409.5-105807								
SW02	ASW000619d	J140522.2+574333	0.7	LQ	✗	✓	✗	✓	✓	10
SW03	ASW0006mea	J142603.2+511421								
SW04	ASW0009cjs	J142934.2+562541	0.5	CQ	✓	✗	✗	✗	✓	74
SW05	ASW0007k4r	J143454.4+522850	0.6	IQ	✓	✓	✓	✓	✓	1.0e+02
SW06	ASW0008swn	J143627.9+563832	0.5	LQ	✗	✓	✓	✓	✗	7
SW07	ASW0007e08	J220256.8+023432								
SW08	ASW00099ed	J020648.0-065639	0.8	D	✓	✓	✗	✓	✓	7
SW09	ASW0002asp	J020832.1-043315	1.0	SQ	✗	✓	✓	✓	✓	9
SW10	ASW0002bmc	J020848.2-042427	0.8	D	✓	✗	✓	✗	✗	3
SW11	ASW0002qtn	J020849.8-050429	0.8	LQ	✗	✓	✗	✓	✓	3
SW12	ASW0003wsu	J022406.1-062846	0.4	D	✓	✓	✗	✓	✓	4
SW13	ASW00047ae	J022805.6-051733	0.4	LQ	✗	✗	✗	✗	✗	7
SW14	ASW0004xjk	J023123.2-082535								
SW15	ASW0004nan	J084841.0-045237	0.3	LQ	✗	✓	✗	✓	✓	8
SW16	ASW0009bp2	J140030.2+574437	0.4	D	✗	✗	✓	✗	✓	5
SW17	ASW0005rnb	J140622.9+520942	0.7	D	✓	✗	✗	✗	✓	6
SW18	ASW0007hu2	J143658.1+533807	0.7	D	✓	✗	✓	✗	✗	4
SW19	ASW0001ld7	J020642.0-095157	0.2	IQ	✗	✓	✗	✗	✓	34
SW20	ASW0002dx7	J021221.1-105251	0.3	IQ	✓	✓	✓	✗	✓	6
SW21	ASW0004m3x	J022533.3-053204	0.5	D	✓	✗	✗	✗	✓	2
SW22	ASW0009ab8	J022716.4-105602	0.4	D		✗	✗	✗	✓	2
SW23	ASW0003r61	J023008.6-054038	0.6	???	?	?	?	?	?	23
SW24	ASW00050sk	J023315.2-042243	0.7	LQ	✗	✓	✗	✓	✓	2
SW25	ASW0007mq	J090308.2-043252								
SW26	ASW0005ma2	J135755.8+571722	0.8	D	✓	✗	✓	✗	✗	9
SW27	ASW0006jh5	J141432.9+534004	0.7	LQ	✗	✗	✗	✗	✓	10
SW28	ASW0007xrs	J143055.9+572431	0.7	LQ	✗	✓	✗	✓	✓	3
SW29	ASW0008qsm	J143838.1+572647	0.8	SQ	✗	✓	✓	✓	✓	4
SW30	ASW0002p8y	J021057.9-084450								
SW31	ASW00021r0	J021514.6-092440	0.7	LQ	✗	✓	✗	✓	✓	24
SW32	ASW0004iye	J022359.8-083651								
SW33	ASW0003s0m	J022745.2-062518	0.6	D	✓	✓	✗	✗	✓	17
SW34	ASW00051ld	J023453.5-093032	0.5	???	?	?	?	?	?	10
SW35	ASW0004wgd	J084833.2-044051	0.8	LQ	✗	✓	✗	✓	✓	5
SW36	ASW000096t	J090248.4-010232	0.4	D	✓	✓	✗	✗	✓	9
SW37	ASW00086xq	J143100.2+564603								
SW38	ASW0009cp0	J143353.6+542310	0.8	LQ	✗	✓	✓	✓	✓	9
SW39	ASW0005qiz	J220215.2+012124								
SW40	ASW0008wmr	J221306.1+014708								
SW41	ASW0008xbu	J221519.7+005758	0.4	IQ	✓	✗	✓	✓	✓	16
SW42	ASW00096rm	J221716.5+015826	0.1	IQ	✓	✓	✗	✓	✗	5.0e+02
SW43	ASW0001c3j	J020810.7-040220	1.0	IQ	✗	✗	✗	✗	✓	6
SW44	ASW0002k40	J021021.5-093415	0.4	???	?	?	?	?	?	34
SW45	ASW00024id	J021225.2-085211	0.8	R	✗	✓	✓	✗	✓	8
SW46	ASW00024q6	J021317.6-084819	0.5	D	✓	✓	✗	✓	✓	6
SW47	ASW0003r6c	J022843.0-063316	0.5	D	✓	✗	✓	✗	✓	26
SW48	ASW0000g95	J090219.0-053923								
SW49	ASW00007ls	J090319.4-040146								
SW50	ASW00008a0	J090333.2-005829								
SW51	ASW0006eo0	J135724.8+561614								
SW52	ASW0006a07	J140027.9+541028								
SW53	ASW00070vl	J141518.9+513915	0.4	D	✓	✗	✓	✗	✓	15
SW54	ASW0007sez	J142620.8+561356	0.5	R	✗	✓	✗	✓	✓	16
SW55	ASW0007t5y	J142652.8+560001								
SW56	ASW0007pga	J142843.5+543713	0.4	D	✓	✗	✓	✗	✗	18
SW57	ASW0008pag	J143631.5+571131	0.7	LQ	✗	✓	✗	✗	✗	64
SW58	ASW0007iwp	J143651.6+530705	0.6	SQ	✗	✗	✓	✓	✓	19
SW59	ASW00085cp	J143950.6+544606								

6 TODO

Todo list

Needs text.	4
Check photometry of this candidate.	7

This paper has been typeset from a T_EX/L_AT_EX file prepared by the author.